Emission times in high-order harmonic generation

C. C. Chirilă,[1] I. Dreissigacker,[1] E. V. van der Zwan,[1,2] and M. Lein[1]

[1]*Centre for Quantum Engineering and Space-Time Research (QUEST) and Institut für Theoretische Physik, Leibniz Universität Hannover, Appelstraße 2, D-30167 Hannover, Germany*

[2]*Institut für Physik, Universität Kassel, Heinrich-Plett-Straße 40, D-31432 Kassel, Germany*

We calculate the emission times of the radiation in high-order harmonic generation using the Gabor transform of numerical data obtained from solving the time-dependent Schrödinger equation in one, two, and three dimensions. Both atomic and molecular systems, including nuclear motion, are investigated. Lewenstein model calculations are used to gauge the performance of the Gabor method. The resulting emission times are compared against the classical simple man's model as well as against the more accurate quantum orbit model based on complex trajectories. The influence of the range of the binding potential (long or short) on the level of agreement is assessed. Our analysis reveals that the short-trajectory harmonics are emitted slightly earlier than predicted by the quantum orbit model. This partially explains recent experimental observations for atoms and molecules. Furthermore, we observe a distinct signature of two-center interference in the emission times for H_2 and D_2.

I. INTRODUCTION

In the past two decades, the high-order harmonic generation (HHG) process [1,2] has been an important subject in both experimental and theoretical physics. Gas-phase HHG occurs when atoms or molecules are irradiated by strong laser pulses, leading to the emission of coherent high-frequency radiation in the soft x-ray regime. It is now frequently used in ultrafast science experiments. Among the increasing number of applications, HHG has been employed for the generation of single attosecond pulses [3] and attosecond pulse trains [4]. The emerging attosecond science [5,6] holds great promise for time-resolved spectroscopy on the attosecond scale. Pulse durations of 130 as were achieved in 2006 [7], and the current record for the shortest pulses is 80 as [8].

Harmonic generation is a nonlinear phenomenon that can be qualitatively explained as a sequence of three steps [9]. First, under the influence of the electric field of the laser pulse, an electron escapes from the atom (molecule) and reaches the continuum. It is subsequently accelerated by the field and driven back toward the atomic (molecular) parent ion. This constitutes the second step. Finally, the electron may recombine with the parent ion. In the recombination step, the kinetic energy accumulated by the electron during its excursion in the continuum, together with the binding energy, is converted into an emitted photon, that is, to harmonic radiation. This essentially classical three-step model [9], also known as the simple man's (SM) model, explains the main features of HHG, such as the existence of a plateau and a cutoff in the emission spectrum. The classical picture emerges elegantly also from the quantum-mechanical description based on the strong-field approximation, known in this context as the Lewenstein model [10]. One of its consequences is that, in order to find the harmonic-emission amplitude at a given photon energy, one needs to sum coherently over a handful of complex electronic trajectories only [11]. These are defined in classical terms, even if they involve complex times. Formally, the conditions defining the trajectories arise from temporal saddle-point approximations [10] and express the energy conservation for the first and third steps described

previously: the energy conservation for the electron emerging from the bound state into the continuum at birth time and the energy conservation for the recombination of the electron with the parent ion under emission of a photon at the return time. Thus, the birth time (or ionization time) t_i and the return time t_r are the complex solutions to the trajectory equations (in atomic units)

$$\frac{[k_s(t_i, t_r) + A(t_i)]^2}{2} = -I_p, \qquad (1)$$

$$\frac{[k_s(t_i, t_r) + A(t_r)]^2}{2} = \Omega - I_p, \qquad (2)$$

where I_p is the ionization potential, $k_s(t', t) = -\int_{t'}^{t} A(t'')dt''/(t - t')$ is the saddle-point electron momentum, Ω is the frequency of the emitted photon, and $A(t)$ is defined by $E(t) = -dA(t)/dt$ with $E(t)$ being the electric field of a linearly polarized laser pulse. We refer to this model as the quantum orbit (QO) model [11]. The real part of the complex return time is interpreted as the physical emission time of the harmonic radiation. If the ionization potential is set to zero in the first step described by Eq. (1), the solution of the saddle-point equations are real times and one arrives at the SM model [9]. For a more in-depth discussion of electronic trajectories, see Ref. [11] and references therein. The QO model implies that the emission time depends on the harmonic frequency, leading to the experimentally confirmed attosecond chirp [12].

The previously mentioned models do not incorporate the influence of the Coulombic attraction of the active electron to the core. This may lead to shortcomings in reproducing *ab initio* results or experimental data. Nevertheless, the three-step model has proven very successful as a basis to explain not only atomic HHG but also molecular aspects of HHG not present in atoms, such as two-center interference effects [13–15] and the influence of the nuclear motion [16–18]. Two-center interference leads to a jump in the harmonic phase at the harmonic order at which the yield is minimal because of destructive interference [13]. Since the emission time is the spectral derivative of the harmonic phase, the phase

jump implies a modification of the emission times, which has been experimentally confirmed [19]. Experimental studies on pairs of isotopes such as (H_2, D_2) permitted gauging clearly the influence of nuclear vibration on the harmonic emission spectra [17,18]. By comparing the harmonic amplitudes in the two isotopes and with the help of quantum-mechanical models, the vibrational motion of the nuclei could be reconstructed from measured data. The reconstruction relies on the one-to-one mapping between harmonic frequencies and electron excursion times provided by the assumption that only the shortest possible trajectory contributes to the harmonic spectrum. Recently, Hässler *et al.* [20] studied experimentally the emission times for HHG from H_2 and D_2, with the intent of establishing whether their measurement can be linked more directly than the harmonic amplitudes to the nuclear dynamics. Earlier, Kanai *et al.* had measured the difference of the harmonic phases in H_2 and D_2 [21]. Both studies suggest small emission time differences between H_2 and D_2, generally much shorter than 100 as.

In a part of the experiments [19,20], an emission-time shift of about 250 as to times earlier than predicted by the QO model, both for atoms and molecules, was observed. The shift has been attributed to an unidentified macroscopic effect in the HHG gas jet. Nevertheless, these measurements and also data from another experiment [8] show that that the attosecond chirp agrees very well with the one from the trajectory models.

In the present work, we retrieve information about harmonic emission times directly from solutions of the time-dependent Schrödinger equation (TDSE) with the help of tools from time-frequency analysis [22]. Such methods have been used before by other authors to obtain the time profile of HHG from atoms; see, for example, Refs. [23–27]. Here we present a systematic study for atoms and molecules. For the latter, we include the nuclear motion in the analysis. Moreover, we inspect the time-frequency structures with finer time resolution than earlier studies.

The major motivation of our work is to investigate in detail the agreement of the emission times from the full quantum-mechanical simulations with the ones from the trajectory models (i.e., the SM model and the QO model). We restrict ourselves to the microscopic single-atom (single-molecule) response. We shed light on the previously mentioned experimentally observed time shift ascribed to macroscopic effects. Our results indicate that a small shift is already found in the single-atom response. Another aim of this work is to investigate the effect of nuclear motion in the isotopes H_2 and D_2 in order to complement the recent experimental work [20,21]. Finally, we investigate the influence of two-center interference on the emission times. This has not been directly calculated before. Despite the fact that a signature reminiscent of two-center interference has been observed experimentally [19], the numerical calculations of the phase behavior [13] have mostly focused on the orientation dependence of the harmonic phase, which is not sufficient to obtain the emission times.

In Sec. II, we revisit the Gabor transformation technique. Then, in Sec. III, we apply the Gabor transformation to obtain the emission times for harmonic spectra calculated from the Lewenstein model for a hydrogenic atom and for the H_2 molecule with inclusion of the vibrational motion. Neither the Lewenstein model nor the QO model takes the effects of the

binding potential fully into account. This means that for atoms, within the frame of the Lewenstein model, any disagreement between the QO emission times and those retrieved from the Gabor transform should be due to the Gabor procedure itself. Furthermore, in the molecular case, another possible reason for disagreement can be the inclusion of the vibrational motion or the two-center interference. In Sec. IV, we proceed with the analysis of the numerical results from the TDSE. We study the influence of the system's dimensionality, compare the tunneling and the multiphoton regimes, and investigate the influence of the range of the binding potential (short or long range). We also analyze the emission times in the isotopes H_2 and D_2. Special attention is given to the influence of the two-center interference. Finally, we present our conclusions in Sec. V. Atomic units are used throughout.

II. GABOR TRANSFORMATION

We estimate the emission times of the harmonic radiation with the help of the Gabor transformation (introduced in the 1940s by D. Gabor [28]), from the time-frequency analysis toolbox. From the dipole acceleration $a(t)$, the harmonic intensity is calculated as the modulus square, $|\tilde{a}(\Omega)|^2$, of its Fourier transform

$$\tilde{a}(\Omega) = \frac{1}{\sqrt{2\pi}} \int dt' \, a(t') \exp(i\Omega t'). \qquad (3)$$

The Gabor transform is defined as

$$a_G(\Omega, t) = \int dt' \, a(t') \, \frac{\exp[-(t' - t)^2/2\sigma^2]}{\sigma\sqrt{2\pi}} \exp(i\Omega t'). \qquad (4)$$

In both Eqs. (3) and (4), the integration is usually taken over the pulse duration. We use here $\sigma = 1/(3\omega_L)$, with ω_L being the central laser frequency. The parameter σ sets the balance between the resolutions in the temporal and frequency domains. In the limit $\sigma \to \infty$, all the temporal information is lost, and the Fourier transform is recovered up to a prefactor that depends on σ. Historically, according to Ref. [22], the Gabor transform has the complex exponential with the opposite sign, that is, $\exp(-i\Omega t')$. For our purpose, however, we choose a functional form similar to the Fourier transform given in Eq. (3). Some authors include an additional multiplication of the Gabor transform with factors that depend on Ω, the analyzed frequency.

The Gabor transform has constant temporal and frequency resolution, irrespective of the harmonic energy studied. In this work, we consider harmonics up to the 55th order at a laser wavelength of 800 nm. The Gabor transform provides satisfactory resolution for the whole harmonic range in all cases studied here, and it is not necessary to consider more sophisticated techniques such as wavelet theory. We plot the modulus squared of the Gabor transform given by Eq. (4). We refer to this type of graph as the Gabor analysis in the following. Alternatively, we plot only the points in time-frequency space where the Gabor amplitude has local maxima for a given frequency. These points can be considered as the emission times for a given harmonic frequency.

In Sec. IV, the shape of the electric field of the laser pulse irradiating the atom or molecule is trapezoidal with two optical cycles turn on and turn off and a plateau with

four optical cycles, and in Sec. III the same trapezoidal shape describes $A(t)$. For the comparison between the Gabor results and the trajectory models, we restrict ourselves to the two shortest possible trajectories for every harmonic frequency since they make the most dominant contribution to the emission spectrum. For our analysis, we choose an emission time interval during the laser pulse for which the complete electron trajectory, from birth time to recombination time, falls within the pulse plateau. In all subsequent figures, the trajectory pair under consideration is represented by the two branches of emission times that merge in the cutoff region at an emission time around 2500 as. Here, the origin of the time axis is placed at the first zero of the electric field in the pulse plateau. For the TDSE calculations, the origin therefore coincides with the beginning of the plateau.

III. RESULTS BASED ON THE LEWENSTEIN MODEL

As a first step, we calculate the harmonic-generation amplitudes from the time-dependent dipole-acceleration expectation value for systems irradiated by a laser pulse. In this section, we employ the Lewenstein model [10] to calculate the dipole acceleration. The model involves an integral over all possible electron momenta for the electron dynamics in the continuum, as well as an integral over all possible times of ionization during the laser pulse. The momentum integration was performed using the saddle-point method, and the integration over the ionization time was performed numerically using the Simpson method. The difference from Ref. [10] is that instead of calculating the dipole moment, we calculate the dipole velocity and differentiate once with respect to time to obtain the dipole acceleration $a(t)$. We refer to this method as the velocity form of the Lewenstein model. It is superior to the usual length form as far as the description of the two-center interference in H_2^+ is concerned [29]. By considering two different laser intensities, both tunneling and multiphoton regimes are investigated. For the two values of the laser intensity, $I = 1.2 \times 10^{14}$ W/cm^2 and $I = 3 \times 10^{14}$ W/cm^2, the Keldysh parameter [30] is $\gamma = 1.07$ (multiphoton regime) and $\gamma = 0.67$ (tunneling regime), respectively, for the laser wavelength 800 nm.

Within the trajectory models, the ionization and emission times are calculated using the SM model, resulting in real times, and within the QO model corresponding to Eqs. (1) and (2), resulting in complex solutions. In the latter case, the real part of the complex return time is regarded as the physical emission time. The Lewenstein model does not take into account the Coulomb interaction in the continuum motion. Therefore, one expects very good agreement between the trajectory models and the Lewenstein model, since the purpose of the Gabor analysis is to reveal the instantaneous frequency components of the dipole acceleration, and those are directly related to the electronic trajectories [10].

Figure 1 shows the calculated emission times for a hydrogenic atom with ionization potential $I_p = 0.6$ a.u. Indeed, the Gabor transformation recovers the electron trajectories, especially in the tunneling regime (right panel). The presence of the well-known short and long trajectory is clearly seen: the emission times smaller than $\sim$2500 as correspond to short trajectories, and the other branch corresponds to the
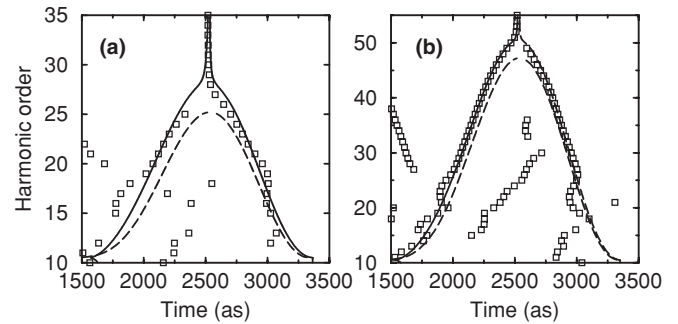

FIG. 1. Emission times for a hydrogenic atom with $I_p = 0.6$ a.u. The dashed (continuous) lines show the emission times from the SM model (QO model). The squares are the emission times obtained from the Gabor analysis of the Lewenstein model results for the harmonic spectrum. (a) Laser intensity $I = 1.2 \times 10^{14}$ W/cm^2 (multiphoton regime); (b) laser intensity $I = 3 \times 10^{14}$ W/cm^2 (tunneling regime).

long trajectories. The highest harmonic orders, that is, the harmonics in the cutoff and beyond, are generated at 2500 as. The SM electron trajectories, in contrast to the results from the QO model, differ significantly from the emission times retrieved by the Gabor transform. The difference between the QO model and the SM model has been noted already in Ref. [11]. The SM model produces a strict cutoff at the harmonic frequency $3.17U_p + I_p$ [9], where U_p is the ponderomotive potential. In Ref. [10], a quantum-mechanical correction has been derived that predicts the cutoff at $3.17U_p + 1.32I_p$. In fact, scaling the ionization potential with the factor 1.32 brings the SM emission times in good agreement with the QO emission times for the harmonics just below the cutoff [26]. However, such a modified SM model remains unable to predict emission times for the harmonics beyond the cutoff and leads to an overcorrection for the low harmonics.

To complete our assessment of the Gabor transformation, we proceed with the case of vibrational motion included in the Lewenstein model [16]. The corresponding numerical simulations presented here are as described in Ref. [16] (without dressing of the molecular ion). In the trajectory models, we use the vertical I_p defined in Ref. [31], which is $I_p = 0.59$ a.u. in the present case. The results are shown in Fig. 2. We notice the good agreement for the short trajectory between the Gabor emission times and the QO emission times. A small temporal shift on the order of 50 as is noticeable; the shift is larger at higher harmonics. An interesting aspect is
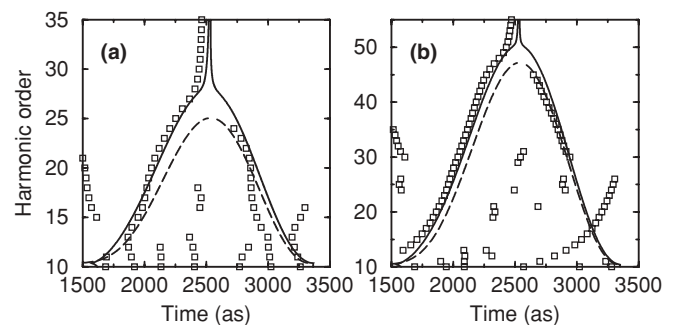

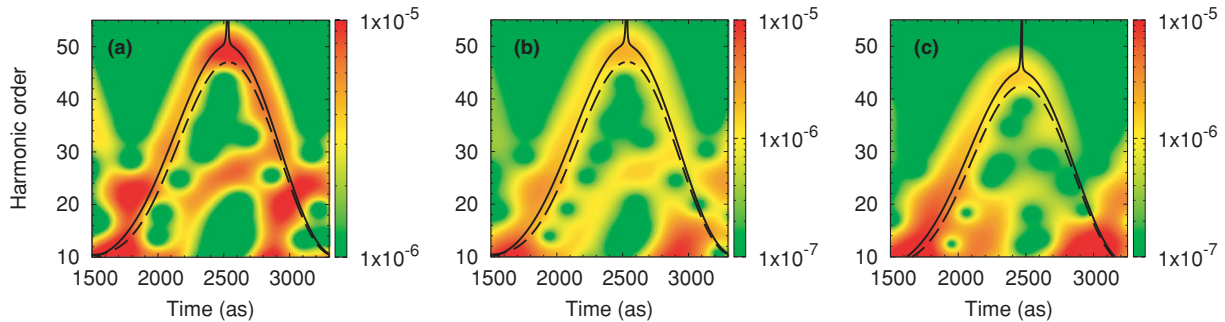FIG. 2. Same as Fig. 1, but for an H_2 molecule with vibrational motion included in the Lewenstein model.

FIG. 3. (Color online) From left to right: the Gabor analysis for HHG from an atom in 1D, 2D, and 3D. In all cases, the binding potential is long range. In the 3D case, the laser wavelength is 780 nm. The dashed (continuous) lines show the emission times from the SM model (QO model). The laser intensity is 3×10^{14} W/cm^2.

that for the long trajectories, there is better agreement with the SM emission times than with the QO ones. This agreement is probably accidental.

We conclude that the QO model gives very good agreement with the Gabor emission times when there is no vibrational motion. When the latter is included, the agreement is still satisfactory, but a small temporal shift appears. One possible reason lies in the fact that the concept of a well-defined ionization potential, which is an essential ingredient of the trajectory models, becomes questionable when a superposition of several vibrational states is formed in the ionization step. The small shift could also be the onset of a two-center interference signature, which is predicted by the Lewenstein model [29] for harmonic orders too high to be completely visible here. See also the discussion in Sec. IV D.

IV. RESULTS BASED ON THE SCHRÖDINGER EQUATION

We solve numerically the TDSE

$$i \frac{\partial \Psi(t)}{\partial t} = [H_0 + x E(t)] \Psi(t) \qquad (5)$$

in one, two, and three dimensions (1D, 2D, and 3D, respectively) for various atomic and molecular systems using the split-operator technique [32]. Here, H_0 is the unperturbed Hamiltonian for the system of interest and $E(t)$ is the time-dependent electric field for a laser pulse polarized along the x axis. Cartesian coordinates are used in the 1D and 2D simulations. In 3D, cylindrical coordinates are used, and the Hankel transformation is used instead of the Fourier transformation to apply the split-operator method to the radial degree of freedom [33]. The dipole acceleration is calculated directly as the expectation value of the gradient of the binding potential [34]. Hereafter, we refer to the results of the Gabor analysis of TDSE simulations as TDSE-Gabor results.

The ionization energy for all atomic and molecular systems considered in this section is $I_p = 0.59$ a.u., except for D$_2$, where I_p differs slightly, and for the 3D hydrogen atom. In detail, the following binding potentials are used: in the 1D case, the short-range potential is taken as $V(x) = -0.992356 \exp(-x^2/2)$ and the long-range potential is $V(x) = -0.894797/\sqrt{1 + x^2}$. In 2D, the short-range potential is $V(x, y) = -2.123344 \exp(-x^2 - y^2)$ and the long-range one is $V(x, y) = -1/\sqrt{0.365494 + x^2 + y^2}$. In 3D, we

study the hydrogen atom using the bare Coulomb potential $V(r) = -1/r$ and the exact reduced electron mass, and the mass is set to one in the reduced-dimensional models, for simplicity. The laser wavelength is 800 nm in all cases except for 3D hydrogen, where 780 nm is used.

In all figures, the solid curves show the emission times from the QO model and the dashed curves show the results from the SM model.

A. Dimensionality of the system

In this section, we study whether the agreement between the Gabor emission times and the SM or QO times is influenced by the problem's dimensionality. To this end, Fig. 3 depicts the Gabor analysis for an atom in 1D, 2D, or 3D. The binding potential is long range.

We conclude that the level of agreement does not depend on dimensionality. The obtained emission times are essentially independent of the number of dimensions. The figure shows that the main influence of the dimensionality is found in the weights of the different trajectories. In the 2D and 3D systems, the degrees of freedom perpendicular to the laser polarization axis allow transverse wave-packet spreading of the returning electron, leading to a suppression of the longer trajectories. The emission times, however, are dictated by the motion of the electron along the polarization axis. In this respect, the other degrees of freedom of the electron motion can be ignored.

The lower-energy structure in Fig. 3, ranging up to approximately the 30th harmonic order with emission times
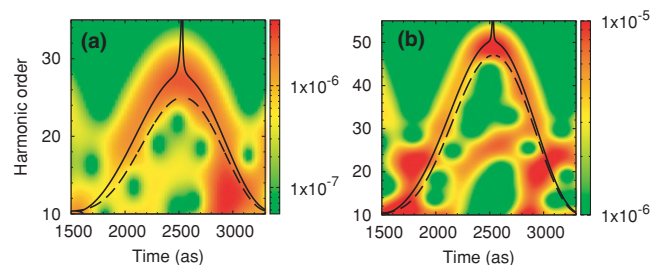

FIG. 4. (Color online) Gabor analysis for HHG from a 1D atom with a long-range binding potential. (a) Laser intensity 1.2×10^{14} W/cm^2 (multiphoton regime); (b) laser intensity 3×10^{14} W/cm^2 (tunneling regime).
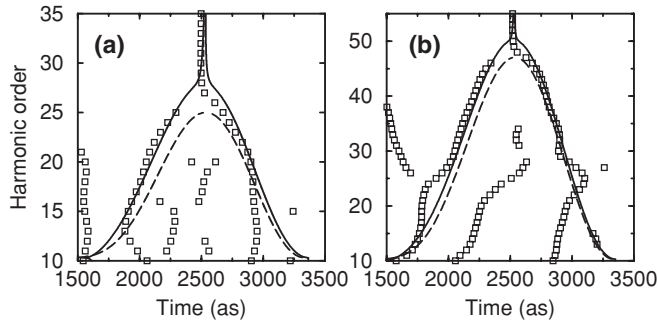
FIG. 5. Emission times obtained from the Gabor analysis in Fig. 4. The empty black squares are the maxima of the Gabor-transform amplitudes.

centered around 2500 as, corresponds to a trajectory pair with travel times longer than those of the shortest trajectory pair.

B. Tunneling and multiphoton regimes

To analyze the influence of the Keldysh parameter, we compare laser intensities that correspond to the multiphoton regime ($\gamma = 1.06 > 1$, left panel of Fig. 4) and tunneling regime ($\gamma = 0.67 < 1$, right panel of Fig. 4). Figure 5 shows the maxima of the Gabor-transform amplitudes from Fig. 4. Overall, the results are very similar to the ones from the Lewenstein model shown in Fig. 1. There is, however, a small but clearly visible shift of the numerical emission times toward earlier times.

In general, at low-order harmonics, the trajectories are not easily distinguishable because of interference in this energy region of more than two trajectories. The Gabor analysis has difficulties in separating frequency components that are too close to each other. Consequently, in this low-frequency range, the SM or QO emission times depart more from the TDSE-Gabor results.

C. Short-range and long-range potentials

In this section, we are concerned with the analysis of the influence of a Coulombic tail on the harmonic emission times. Figure 6 shows the result for a 1D atom, the binding potential of which is taken either short range or long range. Shown are
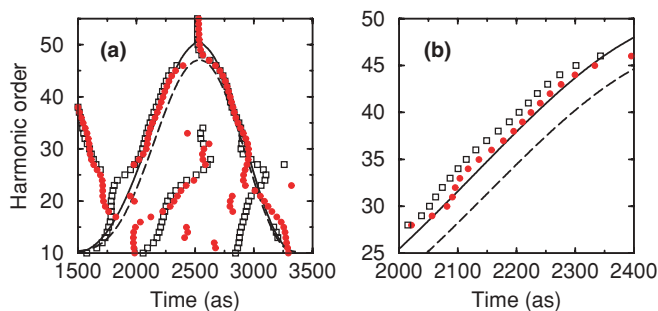

FIG. 6. (Color online) Emission times for a 1D atom. The empty black squares (filled red circles) correspond to a long-range (short-range) binding potential. The laser intensity is 3×10^{14} W/cm^2. The right panel is a magnified view of the short trajectory from the left panel.
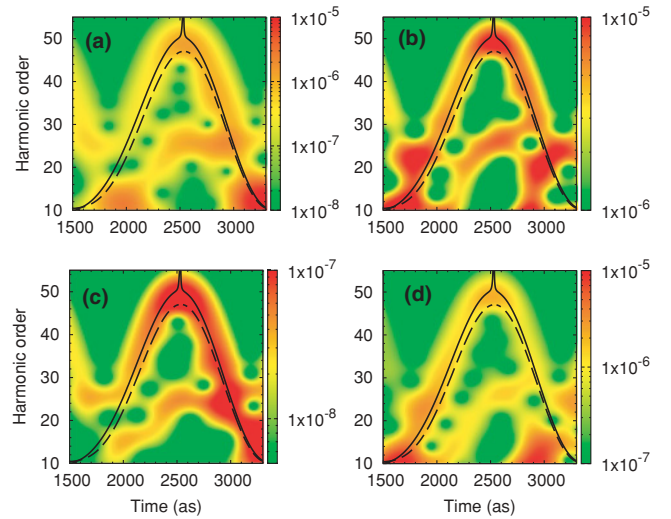

FIG. 7. (Color online) Gabor analysis for various systems. The upper row shows the results for an atom in 1D, and the lower row shows the results for an atom in 2D. Left panels, short-range potential; right panels, long-range potential. The laser intensity is 3×10^{14} W/cm^2.

here the emission times obtained as the maxima of the Gabor-transform amplitudes. The black squares correspond to the long-range binding potential, and the red circles correspond to the short-range potential. The difference between the harmonic emission times in the two binding potentials is about 25 as for the short trajectory, leading to a total emission time shift for the long-range potential of about 30–35 as; see Fig. 6(b).

Figure 7 shows the comparison between short- and long-range potentials, both in 1D and 2D, for an atom. The agreement between the Gabor emission times and the QO values slightly improves in the case of a short-range binding potential, at least for the short trajectory. In all cases, we find excellent agreement for the long trajectory. These reach further away from the atomic core, so that the influence of the binding potential is reduced. For the short trajectory, the influence of the binding potential near the core is expected to be of greater significance, both for short- and long-range potentials. This could explain the small shift visible in the Gabor analysis, which seems to be always present for the short trajectories. Nevertheless, Fig. 6(b) shows that the shift is much smaller for the short-range potential. We thus conclude that the Coulombic tail contributes substantially to the shift toward earlier emission times.
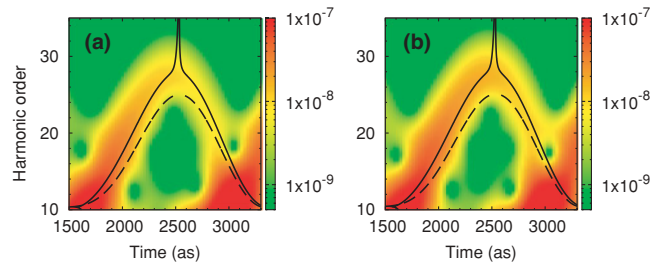

FIG. 8. (Color online) Gabor analysis for HHG from molecules including the vibrational motion. (a) H$_2$; (b) D$_2$. The laser intensity is 1.2×10^{14} W/cm^2.
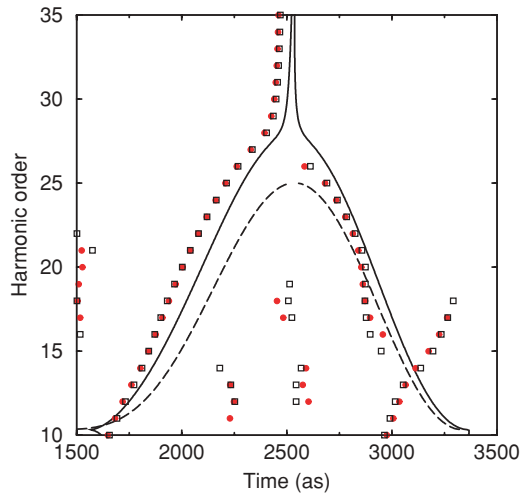
FIG. 9. (Color online) Emission times obtained from the Gabor analysis in Fig. 8. Filled (red) circles, H_2. Empty squares (black), D_2.

D. Molecules

We solve numerically the TDSE for 1D H_2 and D_2 molecules, including the full two-electron dynamics as well as the vibrational motion of the nuclei [35]. The electron-nuclear and electron-electron interaction in the soft-core model is adjusted such that the ground-state Born-Oppenheimer potentials of H_2 and H_2^+ are reproduced [36].

The corresponding Gabor analysis is shown in Fig. 8. The structures that we saw for atoms in the region of low harmonics are suppressed. We attribute this effect to the presence of the vibrational motion, which effectively damps the longer trajectories [16]. As a consequence, the shortest trajectory pair makes the predominant contribution to the harmonic emission. The temporal shift between the QO emission times and the TDSE-Gabor times is now more evident than in the previously studied cases, especially for the short trajectories; see Fig. 9. The presence of an additional shift of ∼50 as in the emission times suggests that the inclusion of nuclear motion modifies the emission times. A similar shift was observed in the Lewenstein result (Fig. 2). As a possible explanation, we pointed out the uncertainty in the value of the ionization potential. However, one may also consider that the two-center interference effect adds its own signature to the emission times, see the case of higher intensity discussed later in this section.

In a recent experiment [20], the difference in harmonic emission times was measured for the pair of isotopes H_2 and D_2. Figure 9 shows that in our calculation the difference
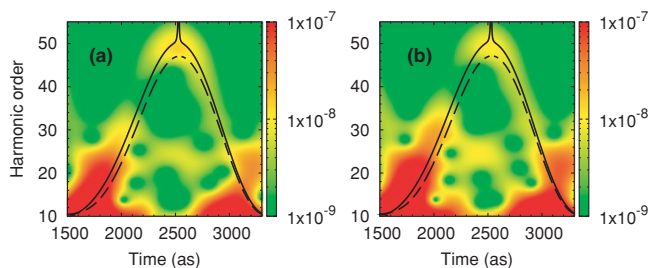

FIG. 10. (Color online) Same as Fig. 8 for the higher laser intensity 3×10^{14} W/cm^2. (a) H_2; (b) D_2.
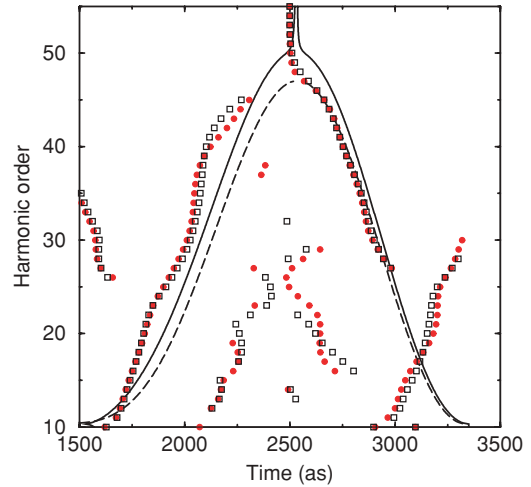
FIG. 11. (Color online) Emission times obtained from the Gabor analysis in Fig. 10. Filled (red) circles, H_2; empty (black) squares, D_2.

between H_2 and D_2 is extremely small: it is of the order of attoseconds. The difference is so small that it is qualitatively and quantitatively sensitive to the temporal width used in the Gabor transform. For this reason, we do not show a plot of the emission-time difference.

Finally, Figs. 10 and 11 show the same analysis but for the higher laser intensity, 3×10^{14} W/cm^2. Apparently, for higher intensities the short-trajectory branch is more structured. As seen before in the last part of Sec. III, the TDSE-Gabor emission times corresponding to the long trajectories agree well with the SM times. In Fig. 10, the amplitude of the Gabor transform is visibly suppressed in the region of the harmonic order 40. This is where the harmonic intensity spectrum undergoes a minimum, due to destructive two-center interference [13]. A hump structure is noticeable in Fig. 11. This is a direct signature of the two-center interference effect. A similar hump structure was observed experimentally by Boutu *et al.* for CO_2 [19]. However, we observe a hump in the opposite direction (i.e, toward earlier times) as compared to the CO_2 experiment. When comparing D_2 and H_2, we find that the hump peaks at lower harmonic orders in H_2. This can be understood as a consequence of the faster nuclear motion in H_2 and thus greater average internuclear distance. The hump around harmonic order 23 is unrelated and comes from contributions of the previous half cycle, as can be seen in Fig. 10.

V. CONCLUSIONS

We have analyzed the emission times in high-order harmonic generation with the help of the Gabor transformation applied to solutions of the time-dependent Schrödinger equation and to data from the Lewenstein model for harmonic generation. We have investigated various atomic and molecular systems with either short- or long-range potentials, and we have studied the effect of the nuclear motion in molecules.

When the electron trajectories responsible for the emission of the harmonics are sufficiently separated, the Gabor transformation is able to isolate efficiently the emission times. When the binding potential is neglected in the continuum

electron motion, as is done in the Lewenstein model, the agreement between the Gabor emission times and the times from the QO model is impressive. Differences appear when going from the tunneling to the multiphoton regime, or when the binding potential (either long- or short-range) is fully taken into account by solving the TDSE. The inclusion of the nuclear motion (either in the Lewenstein model or in the TDSE) produces an additional emission time shift on the order of 50 as, independently of whether H_2 or D_2 is considered. We were not able to predict accurately the tiny emission-time difference in H_2 versus D_2, as such differences appear to be outside the precision range of the Gabor analysis. More theoretical investigations and experimental data are necessary.

We have confirmed the strong modification of the emission times in the region of destructive two-center interference in molecules. However, our calculations for H_2 and D_2 predict a hump in the opposite direction (i.e., toward earlier times) as compared to the experiment on CO_2 [19].

An important conclusion from this work is that there is a generic time shift on the order of 30 as toward earlier times for the short trajectories relative to the predictions of the QO model. Hence, the single-atom (single-molecule) response is responsible for a minor part of the time shift observed in Ref. [20].

Precise knowledge about the timing of the attosecond bursts in harmonic generation is useful for attosecond time-resolved spectroscopy. Moreover, we have shown that the combination of two-center interference and vibrational motion provides a handle to modify fine details of the temporal profile.

[1] A. McPherson *et al.*, J. Opt. Soc. Am. B **4**, 595 (1987).

[2] A. L'Huillier, K. J. Schafer, and K. C. Kulander, J. Phys. B **24**, 3315 (1991).

[3] M. Hentschel *et al.*, Nature **414**, 509 (2001).

[4] P. M. Paul, E. S. Toma, P. Breger, G. Mullot, F. Augé, P. Balcou, H. G. Muller, and P. Agostini, Science **292**, 1689 (2001).

[5] A. Scrinzi, M. Y. Ivanov, R. Kienberger, and D. M. Villeneuve, J. Phys. B **39**, R1 (2006).

[6] F. Krausz and M. Y. Ivanov, Rev. Mod. Phys. **81**, 163 (2009).

[7] G. Sansone *et al.*, Science **314**, 443 (2006).

[8] E. Goulielmakis *et al.*, Science **320**, 1614 (2008).

[9] P. B. Corkum, Phys. Rev. Lett. **71**, 1994 (1993).

[10] M. Lewenstein, P. Balcou, M. Y. Ivanov, A. L'Huillier, and P. B. Corkum, Phys. Rev. A **49**, 2117 (1994).

[11] P. Salières *et al.*, Science **292**, 902 (2001).

[12] Y. Mairesse *et al.*, Science **302**, 1540 (2003).

[13] M. Lein, N. Hay, R. Velotta, J. P. Marangos, and P. L. Knight, Phys. Rev. Lett. **88**, 183903 (2002); Phys. Rev. A **66**, 023805 (2002).

[14] T. Kanai, S. Minemoto, and H. Sakai, Nature **435**, 470 (2005).

[15] C. Vozzi *et al.*, Phys. Rev. Lett. **95**, 153902 (2005).

[16] M. Lein, Phys. Rev. Lett. **94**, 053004 (2005); C. C. Chirilă and M. Lein, Phys. Rev. A **77**, 043403 (2008).

[17] S. Baker *et al.*, Science **312**, 424 (2006).

[18] S. Baker *et al.*, Phys. Rev. Lett. **101**, 053901 (2008).

[19] W. Boutu *et al.*, Nature Phys. **4**, 545 (2008).

[20] S. Hässler *et al.*, J. Phys. B **42**, 134002 (2009).

[21] T. Kanai, E. Takahashi, Y. Nabekawa, and K. Midorikawa, New. J. Phys. **10**, 025036 (2008).

[22] W. C. Lang and K. Forinash, Am. J. Phys. **66**, 794 (1998).

[23] P. Antoine, B. Piraux, and A. Maquet, Phys. Rev. A **51**, R1750 (1995).

[24] C. Figueira de Morisson Faria, M. Dörr, and W. Sandner, Phys. Rev. A **55**, 3961 (1997).

[25] X.-M. Tong and S. I. Chu, Phys. Rev. A **61**, 021802(R) (2000).

[26] V. S. Yakovlev and A. Scrinzi, Phys. Rev. Lett. **91**, 153901 (2003).

[27] A. Pukhov, S. Gordienko, and T. Baeva, Phys. Rev. Lett. **91**, 173002 (2003).

[28] D. Gabor, J. Inst. Electr. Eng. **93**, 429 (1946).

[29] C. C. Chirilă and M. Lein, J. Mod. Opt. **54**, 1039 (2007).

[30] L. V. Keldysh, Zh. Eksp. Teor. Fiz. **47**, 1945 (1964)[Sov. Phys. JETP **20**, 1307 (1965)].

[31] C. C. Chirilă and M. Lein, J. Phys. B **39**, S437 (2006).

[32] M. D. Feit, J. A. Fleck Jr., and A. Steiger, J. Comput. Phys. **47**, 412 (1982).

[33] L. Yu, M. Huang, M. Chen, W. Chen, W. Huang, and Z. Zhu, Opt. Lett. **23**, 409 (1998).

[34] K. Burnett, V. C. Reed, J. Cooper, and P. L. Knight, Phys. Rev. A **45**, 3347 (1992).

[35] C. C. Chirilă and M. Lein, Chem. Phys. **366**, 54 (2009).

[36] S. Saugout, C. Cornaggia, A. Suzor-Weiner, and E. Charron, Phys. Rev. Lett. **98**, 253003 (2007).